Surface Solar Extremes in the Most Irradiated Region on Earth, Altiplano

Raúl R. Cordero[iD], Sarah Feron, Alessandro Damiani, Edgardo Sepúlveda, Jose Jorquera, Alberto Redondas, Gunther Seckmeyer, Jorge Carrasco, Penny Rowe, and Zutao Ouyang

ABSTRACT: Satellites have consistently pointed to the Altiplano of the Atacama Desert as the place on Earth where the world's highest surface irradiance occurs. This region, near the Tropic of Capricorn, is characterized by its high elevation, prevalent cloudless conditions, and relatively low concentrations of ozone, aerosols, and precipitable water. Aimed at studying the variability of the surface solar irradiance and detecting atmospheric composition changes in the Altiplano, an atmospheric observatory was set up in 2016 at the northwestern border of the Chajnantor Plateau (5,148 m MSL, 22.95°S, 67.78°W, Chile). Here, we report on the first 5 years of measurements at this observatory that establish the Altiplano as the region that receives the highest-known irradiation on Earth and illuminate the unique features of surface solar extremes at high-altitude locations. We found that the global horizontal shortwave (SW) irradiance on the plateau is on average 308 W m^{-2} (equivalent to an annual irradiation of 2.7 MWh m^{-2} yr^{-1}, the highest worldwide). We also found that forward scattering by broken clouds often leads to intense bursts of SW irradiance; a record of 2,177 W m^{-2} was measured, equivalent to the extraterrestrial SW irradiance expected at approximately 0.79 astronomical units (AU) from the Sun. These cloud-driven surface solar extremes occur on the Chajnantor Plateau at a frequency, intensity, and duration not previously seen anywhere in the world, making the site an ideal location for studying the response of photovoltaic (PV) power plants to periods of enhanced SW variability.

KEYWORDS: Atmosphere; South America; Extreme events; Shortwave radiation; Surface observations; Renewable energy

AFFILIATIONS: **Cordero and Jorquera**—Universidad de Santiago de Chile, Santiago, Chile; **Feron**—Universidad de Santiago de Chile, Santiago, Chile, and University of Groningen, Leeuwarden, Netherlands; **Damiani**—Center for Climate Change Adaptation, National Institute for Environmental Studies, Tsukuba, Japan; **Sepúlveda**—Universidad de Santiago de Chile, Santiago, Chile; **Redondas**—State Meteorological Agency (AEMET), Santa Cruz de Tenerife, Spain; **Seckmeyer**—Leibniz Universität Hannover, Hannover, Germany; **Carrasco**—University of Magallanes, Punta Arenas, Chile; **Rowe**—NorthWest Research Associates, Seattle, Washington; **Ouyang**—Stanford University, Stanford, California

S olar radiation is the ultimate energy source for the Earth's biosphere, and the driving force for atmospheric and oceanic circulation. The spectrally integrated energy input to the top of the Earth's atmosphere at one astronomical unit (AU) is referred to as the total solar irradiance (TSI), once known as the "solar constant" (Dudok de Wit et al. 2017). Most of the surface irradiance, which corresponds to the fraction of the TSI that passes through the atmosphere to the Earth's surface, is within the shortwave (SW) range (0.29–3 μm) (Loeb et al. 2016).

Continuous observations of the surface SW irradiance enable the detection of climate responses on different time scales as well as atmospheric composition changes; the fingerprint left on the spectral SW irradiance by atmospheric absorption and scattering processes allows retrieving information about the atmospheric constituents (such as gaseous concentrations, aerosols, and clouds) (Kratz et al. 2020). Quality-controlled ground-based measurements are of primary importance for the validation of radiative transfer calculations and satellite estimates (Kratz et al. 2020; Rutan et al. 2015).

Observations of the surface SW irradiance are also a key tool for assessing the solar energy potential. Carbon-free solar electricity generation is expected to play a major role in reducing global emissions and mitigating climate change. Long-term records of the SW irradiance incident on a horizontal plane [often referred to as global horizonal irradiance (GHI)] provide a direct and harmonized assessment of the available solar resources (Prăvălie et al. 2019). These records have shown that around 20% of the global population lives in 70 countries with excellent conditions for solar energy projects (ESMAP 2020).

Due to its high elevation and proximity to the equator, the Atacama Desert stands out among other major solar hotspots. The global horizontal SW irradiance, which is on average about 240 W m^{-2} on the Tibetan Plateau (Gelsor et al. 2018), climbs to about 275 W m^{-2} in the Atacama Desert, and peaks at values close to 300 W m^{-2} in the Altiplano (Prăvălie et al. 2019; Yang and Bright 2020). With an average elevation of about 3,750 m MSL, the Altiplano is the widest part of the Andes Mountain range, consisting of several connected basins in northern Chile, western Bolivia, southern Peru, and northwest Argentina. The thin atmosphere and low concentrations of absorbers and scatterers favor extremely high clear-sky SW irradiance in the Altiplano region (Cordero et al. 2016; Rondanelli et al. 2015) (Fig. S1 in the online supplemental material).

According to NASA's CERES Energy Balanced and Filled (EBAF) data (NASA/LARC/SD/ASDC 2019) (see appendix A), the world's highest surface SW irradiance occurs in the Altiplano of the Atacama Desert, very close to the Chajnantor Plateau (Fig. 1a). This vast flat expanse of about 50 km^2 has been used since immemorial times for worshipping the Sun; in Kunza, the ancestral language of the people living in the region, Chajnantor means "lift-off place"
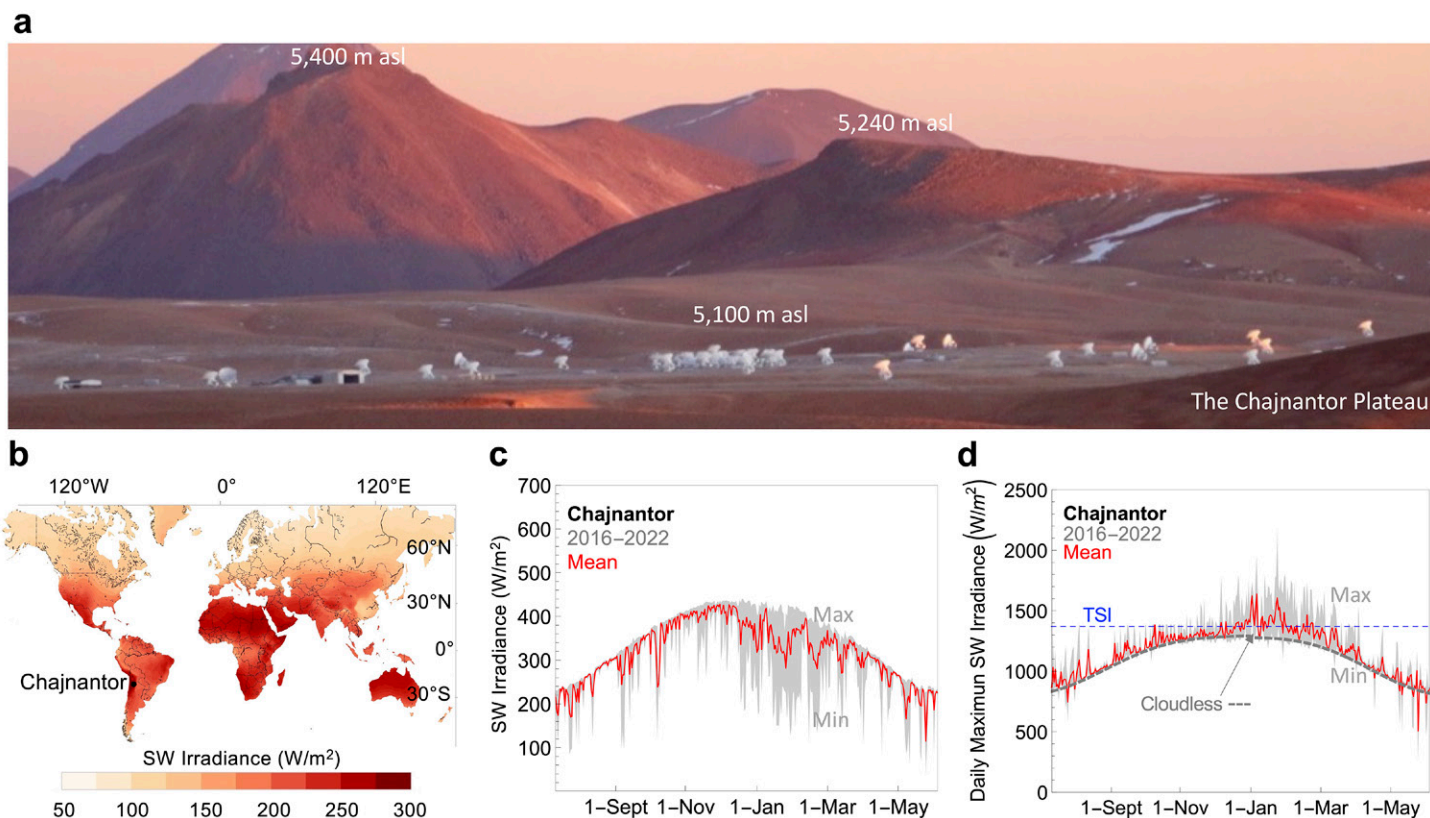
Fig. 1. The world's highest surface solar irradiance occurs on the Chajnantor Plateau. (a) Chajnantor Plateau (5,100 m MSL, 23.00°S, 67.75°W) in the Atacama Desert. The vast flat expanse of about 50 km² hosts major astronomical projects including the Atacama Large Millimeter/Submillimeter Array (ALMA). Picture by the authors. **(b)** Annual mean surface SW irradiance computed over the period 2011–20 from NASA's CERES Energy Balanced and Filled (EBAF) data (NASA/LARC/SD/ASDC 2019). The satellite-derived CERES-EBAF data are used for climate model evaluation and for estimating the Earth's global mean energy budget. According to the 1°-resolution CERES-EBAF dataset, the grid point (23.5°S, 67.5°W) that includes the Chajnantor Plateau experiences the highest annual mean surface SW irradiance globally (302 W m⁻²). **(c)** Daily mean surface SW irradiance measured at Chajnantor using a SMP-21 Kipp and Zonen pyranometer. The gray shading indicates the highest and lowest values measured for each day of year (DOY) over the period 2016–22 while the red line indicates the mean over the same period. According to our measurements, the annual mean of the surface SW irradiance at Chajnantor is 308 W m⁻², which roughly agrees with CERES-EBAF estimate (302 W m⁻²). **(d)** Daily maximum surface SW irradiance measured at Chajnantor. The gray shading indicates the highest and lowest values measured for each day of year (DOY) over the period 2016–22. Our 1-min measurements at Chajnantor show that the daily maximum surface SW irradiance often exceed the expected clear-sky SW ceiling (computed using a radiative transfer model) and sometimes also the Total Solar Irradiance (approximately 1,362 W m⁻²) (Dudok de Wit et al. 2017). Unless otherwise indicated, plots in this paper were generated using Python's Matplotlib library (Hunter 2007).

(ESO 2007). The mean temperature on the Plateau, usually around 0°C in summer, drops considerably up to around −6°C in winter when gusty winds over 15 m s⁻¹ are more frequent (Fig. S2). Chajnantor hosts major astronomical projects including the Atacama Large Millimeter/Submillimeter Array (ALMA) (ESO 2007).

Aimed at studying the variability of the surface solar irradiance and detecting atmospheric composition changes in the Altiplano region, an atmospheric observatory was set up in 2016 at the northwestern border of the Chajnantor Plateau (5,148 m MSL, 22.95°S, 67.78°W, Chile, Fig. S3). The Chajnantor Observatory, the Nepal Climate Observatory-Pyramid (NCO-P, at 5,079 m MSL, 27.96°N, 86.81°E, in the Khumbu Valley near Mt. Everest) (Marcq et al. 2010), and the Chacaltaya Observatory (CHC, at 5,240 m MSL, 16.35°S, 68.13°W, near the Chacaltaya summit in the Bolivian Altiplano) (Aliaga et al. 2021) are the only atmospheric research facilities above 5,000 m MSL in the world. Collaud Coen et al. (2018) provide a comprehensive list of high-altitude research stations around the globe.

Here, we report on 5 years of measurements of the SW irradiance at the Chajnantor Observatory (see appendix B). Broadband measurements were made with a Class A

pyranometer (SMP-21, Kipp and Zonen), while quality-controlled spectral measurements in the ultraviolet (UV), visible, and part of the infrared range were conducted using a spectro-radiometer system that fulfills specifications of the Network for the Detection of Atmospheric Composition Change (NDACC) (Wuttke et al. 2006) and the World Meteorological Organization (WMO) (Seckmeyer et al. 2001). Additional ground-based spectral measurements involved photometers affiliated with the Aerosol Robotic Network (AERONET) (Holben 1998) and SKYNET (Nakajima et al. 2020). Estimates of the total ozone column (TOC), the total precipitable water (TPW), and the aerosol optical depth (AOD) were retrieved from our spectral measurements. For complementary radiative transfer calculations, we used the libRadtran software package (Mayer and Kylling 2005).

Results

Our measurements have validated satellite estimates that pointed to the Altiplano of the Atacama Desert as the most irradiated region on Earth. The Chajnantor Plateau lies within the grid point where, according to the NASA's CERES-EBAF data (NASA/LARC/SD/ASDC 2019), the world's highest surface irradiance occurs (Fig. 1b). According to our ground-based measurements, the annual mean of the surface SW irradiance at the Chajnantor Observatory is 308 W m^{-2} (Fig. 1c), which roughly agrees with the CERES-EBAF estimate (302 W m^{-2}).

Due to its proximity to the equator, the annual irradiation is considerably higher on the Altiplano of the Atacama Desert than in other high-altitude regions, for example, the Tibetan Plateau. The annual mean of the surface SW irradiance at Chajnantor (308 W m^{-2}) is equivalent to an annual irradiation of 2.7 MWh m^{-2} yr^{-1}, which is well above (about 28%) the annual irradiation measured at Lhasa (3,683 m MSL, Tibet) (Gelsor et al. 2018). The elevation of Chajnantor (about 1,400 m higher than Lhasa) accounts for a relatively small fraction (about one-fifth) of the differences in annual irradiation; most of the differences in annual irradiation are attributable to the lower latitude of Chajnantor with respect to Lhasa (23.0°S versus 29.6°N).

The differences between Chajnantor and high-altitude locations on the southern Tibetan Plateau are smaller when comparing annual maximum SW irradiances (i.e., measured when the Sun reaches its annual maximum elevation). On the Chajnantor Plateau, the solar zenith angle (SZA) is almost 0° on the summer solstice, while on the southern Tibetan Plateau (28°N) it reaches a minimum of about 5° close to the summer solstice. At high-altitude sites, where the aerosol load is generally low, small differences in the SZA (0° versus 5°) lead to small differences in the SW irradiances (about 2% higher on the Chajnantor Plateau than on the Tibetan Plateau). These relatively small differences are considerably amplified by the fact that the austral summer occurs when the Earth's orbit is closer to the Sun (i.e., perihelion occurs in early January), which makes the summer clear-sky SW irradiances up to 7% higher in the Southern Hemisphere than in the Northern Hemisphere. Although the elevation of the peaks on the Tibetan Plateau (3,000 m higher than Chajnantor) may offset most of the differences (Fig. S4), the noontime SW irradiance has nonetheless been found to be slightly higher at Chajnantor than at the world's highest sites. While the summer daily maximum SW irradiance measured under cloudless conditions at Chajnantor is close to 1,280 W m^{-2} (Fig. 1d), the noontime SW irradiance measured at South Col (close to the summit of Mount Everest, 28°N, 7,945 m MSL) is around 1,250 W m^{-2} (Matthews et al. 2020).

Although elevation and proximity to the equator play a major role, the thin atmosphere and low concentrations of absorbers and scatterers also favor the clear-sky SW extremes on Chajnantor Plateau (Fig. 2). The TOC, AOD, and TPW are considerably lower over the Atacama Desert than over other regions of high solar potential (Cordero et al. 2016). For example, AOD values in the Atacama Desert are on average about half of those observed in northwestern Africa (Wei et al. 2019). According to our ground-based measurements, the annual means on
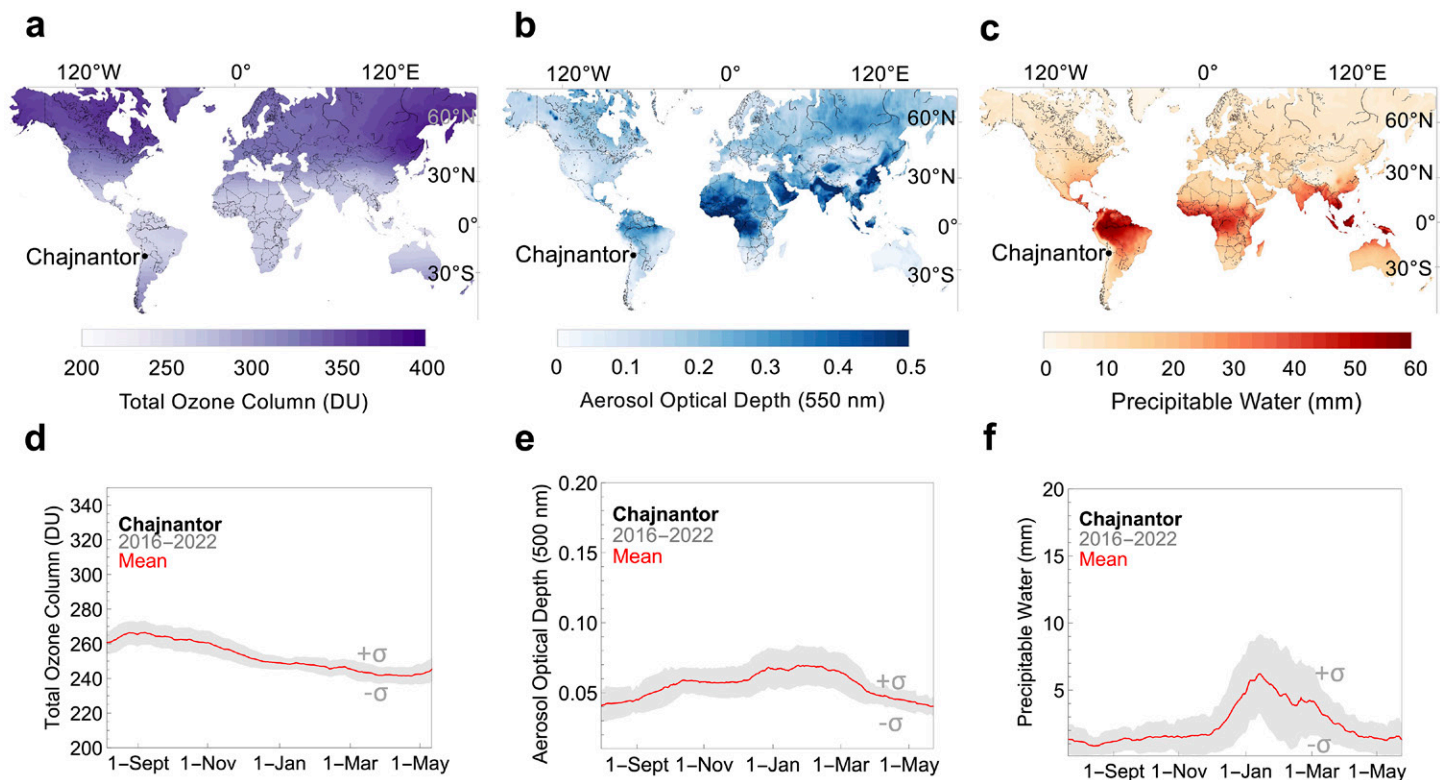
Fig. 2. The thin atmosphere favors the extremely high surface radiation on the Chajnantor Plateau. (a),(d) Total ozone column (TOC); (b),(e) aerosol optical depth (AOD); and (c),(f) total precipitable water (TPW). (top) Annual mean of satellite-derived estimates over the period 2011–20. TOC data are from the Ozone Monitoring Instrument (OMI) Differential Optical Absorption Spectroscopy (OMI-DOAS) on board the *Aura* satellite (Veefkind 2012) while AOD and PW data are from the level-3 Moderate Resolution Imaging Spectroradiometer (MODIS) on board the *Aqua* satellite (Platnick et al. 2015). According to satellite estimates, the annual means on the Chajnantor Plateau of TOC, AOD, and TPW are 256 DU, 0.06, and 2.7 mm, respectively. (bottom) Ground-based measurements at the Chajnantor Observatory over the period 2016–22. For each day of year (DOY), we used a 29-day rolling window to form datasets of the available measurements. The mean and standard deviation (σ) of these datasets are shown in plots (d)–(f). According to our measurements, the annual means at the Chajnantor Observatory of TOC, AOD, and TPW are 255 DU, 0.05, and 2.4 mm, respectively.

the Chajnantor Plateau of TOC, AOD, and PW are 255 Dobson units (DU), 0.05, and 2.4 mm, respectively. In contrast to TOC (Fig. 2d) and AOD values (Fig. 2e), TPW values at Chajnantor exhibit a considerable seasonality (Fig. 2f). The atmosphere above the Chajnantor Plateau is the second driest in the world (after Antarctica). However, the South American monsoon (Carvalho et al. 2012) enhances moisture transport from the Amazon basin leading to seasonal changes in the TPW on the Chajnantor Plateau. Although the summer TPW rise shown in Fig. 2f can reduce the clear-sky SW irradiance by up to 3%, monsoon-boosted moisture can lead to much larger changes in SW irradiance if it condenses forming clouds.

The unique features of the Chajnantor Plateau include the so-called cloud enhancement events (i.e., intense bursts of SW irradiance far exceeding expected clear-sky values and often extraterrestrial levels). While clouds generally attenuate the surface radiation by preventing it from reaching the surface, forward scattering by clouds of suitable type and optical thickness can enhance the global horizonal irradiance (Damiani et al. 2018; Gueymard 2017; Piedehierro et al. 2014; Yordanov et al. 2015). Strong forward scattering can boost the global horizonal irradiance well above the clear-sky ceiling (Piedehierro et al. 2014; Yordanov et al. 2015). Although an upper limit is still uncertain, simulations of the radiative transfer through a cloudy atmosphere suggests that cloud enhancement by a factor of about 1.8 (with respect to the expected clear-sky SW irradiance) is possible (Yordanov et al. 2015). Yordanov et al. (2015) estimated that extremes higher than 2,000 W m^{-2} are likely at latitudes within ±30° around the equator. As discussed below, our measurements confirm this estimation.

Table 1. Top-10 SW extremes observed at Chajnantor since 2016 (shaded) compared with prior top-10 records registered elsewhere by using pyranometers. Additionally, SW Irradiances of up to 1.6 KW m⁻² have been measured by using other sensors in São Paulo (southern Brazil) (Almeida et al. 2014) and in Grimstad (southern Norway) (Yordanov et al. 2015). Note that the all-time record of 2,177 W m⁻² is equivalent to the extraterrestrial SW irradiance expected at approximately 0.79 AU from the Sun (as a reference, Venus is 0.73 AU at its farthest distance from the Sun).

SW irradiance (W m^{-2})	Location	Elevation (m)	Resolution (s)	Instrument	Date or reference
2,177	Chajnantor, Chile	5,148	60	SMP21 pyranometer	24 Jan 2017
1,952	Chajnantor, Chile	5,148	60	SMP21 pyranometer	6 Jan 2021
1,891	Colorado, United States	1,829	1	LICOR LI-200	Gueymard (2017)
1,872	Chajnantor, Chile	5,148	60	SMP21 pyranometer	6 Jan 2020
1,845	Caucaia, Brazil	32	1	SPN1 pyranometer	do Nascimento et al. (2019)
1,832	Andean Mountains, Ecuador	3,400	300	CM3 pyranometer	Emck and Richter (2008)
1,805	Chajnantor, Chile	5,148	60	SMP21 pyranometer	31 Jan 2017
1,796	Chajnantor, Chile	5,148	60	SMP21 pyranometer	21 Dec 2021
1,795	Chajnantor, Chile	5,148	60	SMP21 pyranometer	31 Jan 2017
1,782	Chajnantor, Chile	5,148	60	SMP21 pyranometer	23 Jan 2017
1,780	Chajnantor, Chile	5,148	60	SMP21 pyranometer	22 Jan 2020
1,780	Chajnantor, Chile	5,148	60	SMP21 pyranometer	5 Jan 2021
1,779	Chajnantor, Chile	5,148	60	SMP21 pyranometer	6 Jan 2021
1,691	Carrera Pinto, Atacama Desert	1,920	60	LICOR LI-200	Castillejo-Cuberos and Escobar (2020)
1,543	Lima, Peru	54	1–3	EKO MS-80	Jara et al. (2021)
1,533	Cyprus	360	60	MS-802 pyranometer	Tapakis and Charalambides (2014)
1,528	Puna of Atacama, Argentina	3,900	5	PSP Eppley pyranometer	Piacentini et al. (2003)
1,477	Recife, Brazil	4	60	CM11 pyranometer	Piacentini et al. (2011)
1,466	San Diego, United States	118	2	LICOR LI-200	Lappalainen and Kleissl (2020)
1,450	Lauder, New Zealand	370	60	BSRN-certified pyranometer	Pfister et al. (2003)

Powered by cloud enhancements, 7 of the highest 10 SW extremes on record around the world have occurred on the Chajnantor Plateau (Table 1) (see appendix C). Our ground-based measurements show that the daily maximum SW irradiance at Chajnantor frequently exceeds both the clear-sky ceiling and the TSI (Fig. 1d). Although values of the SW irradiance higher than the TSI have also been also measured elsewhere, SW extremes detected at Chajnantor stand out from the rest (Table 1). On 24 January 2017, we measured the highest global horizontal SW irradiance ever registered: 2,177 W m⁻², a value considerably higher than prior records from the United States (Gueymard 2017), Brazil (do Nascimento et al. 2019), and Ecuador (Emck and Richter 2008), which all fell below 1,900 W m⁻² (Table 1). Satellite imagery from *GOES-16* (band 4, 1.37 μm, Near-IR, "Cirrus Band," Fig. S5) suggest the presence of cumuliform (Sc/Cu) and cirrus clouds over the Chajnantor (Ch) Plateau on 24 January 2017. Prior efforts (e.g., Cede et al. 2002; Castillejo-Cuberos and Escobar 2020) have shown that cloud enhancement occurs frequently with cumulus-type clouds (cumulus, stratocumulus, altocumulus, and cirrocumulus), as well as with cirrus or cirrostratus clouds. The synoptic-scale circulation shows that easterly winds prevailed over the Altiplano that day, which are conditions typically associated with the South American monsoon (Carvalho et al. 2012).

Although cloudless conditions prevail most of the time in the Atacama Desert (Fig. S6), the South American monsoon (Carvalho et al. 2012) makes clouds more frequent on the Chajnantor Plateau during mid- and late summer (January and February). The effect of clouds on the surface solar radiation is often characterized by the cloud modification factor (CMF), generally defined as the ratio between the measured all-sky surface radiation and the

corresponding clear-sky surface radiation computed using a radiative transfer model (Staiger et al. 2008). According to our measurements (Fig. 3a), the annual mean of the daily CMF values at Chajnantor is higher than 0.9 (i.e., clouds attenuate the daily SW irradiation by less than 10%). However, attributable to the thicker and frequent clouds, daily CMF values are considerably lower than 0.9 in mid- and late summer.

Summertime cloud conditions on the Chajnantor Plateau not only favor short-lived SW extremes but also often lead to persistent cloud enhancement events. Prior efforts elsewhere have shown that cloud enhancement events can last from seconds and minutes (Tapakis and Charalambides 2014) to, occasionally, hours (Cede et al. 2002). At Chajnantor, we have registered cloud enhancement events lasting up to 4 h. The all-time SW record (2,177 W m^{-2}) on 24 January 2017 was in fact preceded by a cloud enhancement event that lasted about 3 h, from midmorning to about noon (Fig. 3b). The surface SW irradiance repeatedly exceeded clear-sky levels during the afternoon when 1-min-resolution CMF values (computed dividing our all-sky 1-min SW measurements by the corresponding clear-sky SW estimates) ranged from 0.2 close to the sunset to 1.7 close to noon (Fig. 3c). If considered sequentially, cloud enhancement lasted 226 min on 24 January 2017.

According to our measurements, cloud enhancement events occur on the Chajnantor Plateau at a frequency, intensity, and duration not previously measured anywhere in the world:

- Cloud enhancement events at Chajnantor are so frequent that the daily probability of detecting such an event using 1-min-resolution measurements is on average close to 0.5 (gray line in Fig. 3d). Attributable to the thicker and frequent clouds, enhancement events are slightly more frequent in mid- and late summer.
- The probability of the daily maximum SW irradiance at Chajnantor surpassing extraterrestrial levels is higher than 0.5 in January (blue line in Fig. 3d). Due to the concurrence of frequent broken cloud conditions and high solar elevations (occurring just a few weeks after the summer solstice), the daily maximum SW irradiance at Chajnantor is on average higher than the TSI during January (Fig. 1d).
- The daily maximum cloud enhancement at Chajnantor is on average about 1.3 (Fig. 3e) but enhancements close to the 1.8 [the upper limit suggested by models (Yordanov et al. 2015)] have been registered. The all-time record of surface SW irradiance (2,177 W m^{-2}) resulted from an enhancement of about 1.7 (corresponding to more than 850 W m^{-2}, Figs. 3b,c).
- Cloud enhancement events at Chajnantor last on average 12 min in total per day (Fig. 3f), although we have registered events that lasted for hours (Fig. 3c). Attributable to the thicker and more frequent clouds, enhancement durations nearly triple in mid- and late summer with respect to the rest of the year (Fig. 3f). If considered sequentially, cloud enhancement events at Chajnantor last more than 6 days yr^{-1}, which is nearly twice the total duration observed elsewhere (Inman et al. 2016).

The Chajnantor Plateau is also where the world's highest surface UV irradiance occurs. Satellite estimates have consistently indicated that the UV index (i.e., a proxy of the erythemally active UV irradiance) on the Altiplano is the highest worldwide (Fig. 4a), with a peak of almost 20. In agreement with satellite estimates, our ground-based measurements show that the summer daily maximum UV index at Chajnantor is also on average slightly lower than 20 (Fig. 4b). Some of the factors that favor SW records (elevation and proximity to the equator) also contribute to the extreme UV levels observed at Chajnantor. However, in the case of the UV irradiance, the low ozone column over the Atacama Desert plays a major role (Fig. 2a). TOC values are on average about 10% lower over the Atacama Desert than over
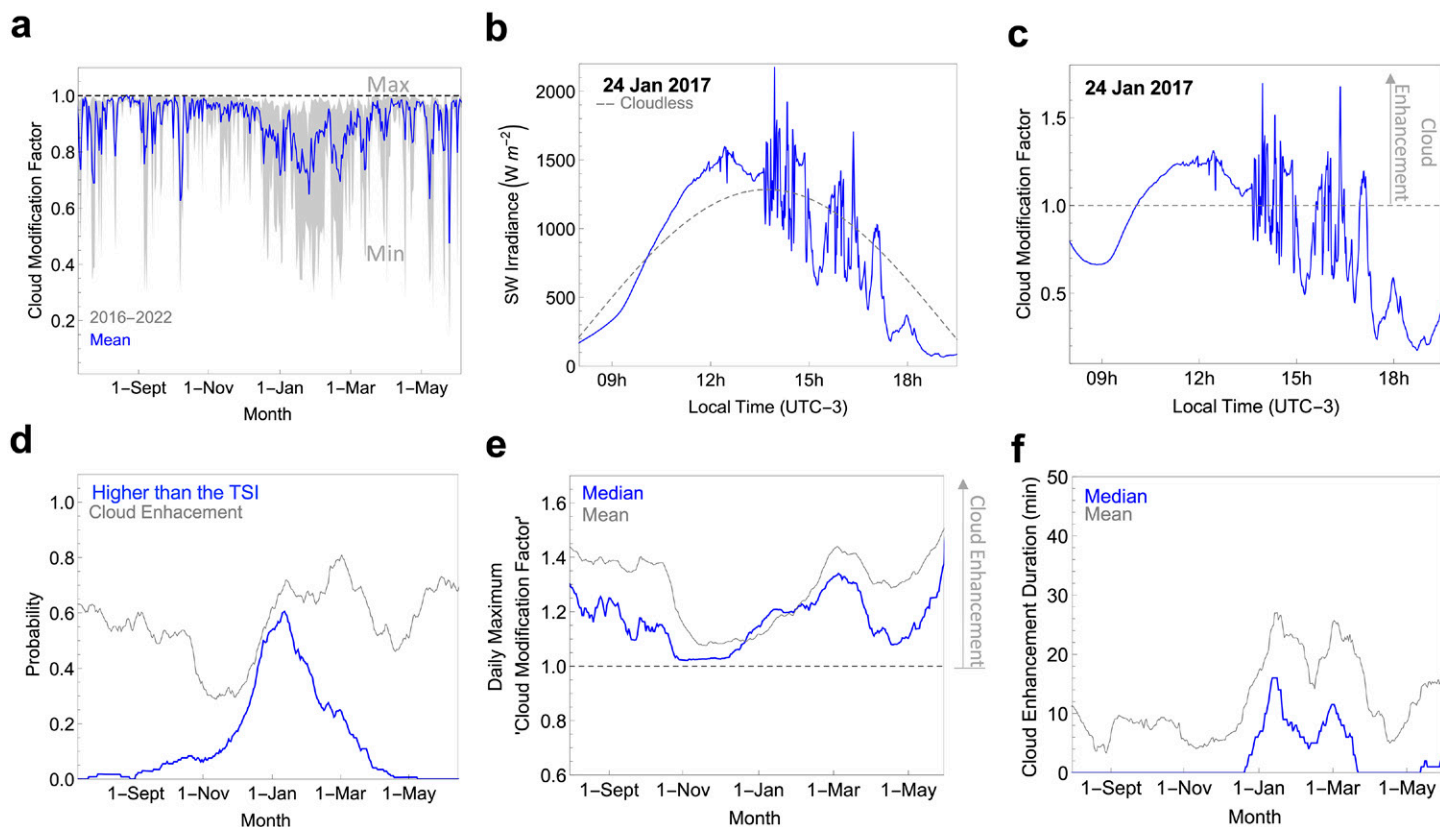
Fig. 3. Broken cloud conditions on the plateau often lead to bursts of surface solar irradiance far exceeding clear-sky levels. (a) 1-day cloud modification factor (CMF): ratio between the daily all-sky SW irradiation measured at Chajnantor and the corresponding daily clear-sky SW irradiation computed using a radiative transfer model. The gray shading indicates the highest and lowest 1-day CMF values over the period 2016–22 while the blue line indicates the mean over the same period. The annual mean of the CMF at Chajnantor is higher than 0.9 (although lower values are frequent in mid- and late summer). **(b)** 1-min all-sky SW irradiance measured at Chajnantor on 24 Jan 2017 (solid blue line) and the corresponding clear-sky SW irradiance computed using a radiative transfer model (dashed gray line). Although clouds generally attenuate the surface irradiance (i.e., CMF values are generally lower than 1), our measurements at Chajnantor show that forward scattering by broken clouds on 24 Jan 2017 led to all-sky SW values far exceeding clear-sky levels (i.e., CMF values higher than 1). **(c)** 1-min CMF computed using the data shown in (b). We calculated the 1-min-resolution CMF values dividing our all-sky SW irradiance measurements at Chajnantor by the corresponding clear-sky SW irradiance computed using a radiative transfer model. CMF values lower than 1 were observed in early morning and late afternoon. However, cloud conditions prevalent from about 10 h to about 13 h led to CMF values higher than 1 (i.e., cloud enhancement) for several hours. Although rare elsewhere, cloud enhancement occurs on the Chajnantor Plateau at a frequency, intensity, and duration not seen anywhere in the world. **(d)** Probability of the daily maximum SW irradiance at Chajnantor being higher than the TSI (blue line) for at least 1 min, and probability of cloud enhancement being higher than 1.1 for at least 1 min (gray line). The latter is equivalent to the all-sky SW irradiance at Chajnantor being at least 10% higher than clear-sky levels for at least 1 min. **(e)** Daily maximum CMF observed on the Chajnantor Plateau: median (blue line) and mean (gray line). CMF values higher than one indicate cloud enhancement. Although we have registered cloud enhancements close to 1.8, the daily maximum cloud enhancement at Chajnantor is on average about 1.3. **(f)** Cloud enhancement duration: median (blue line) and mean (gray line) of the number of minutes a day that the all-sky SW irradiance is at least 10% higher than clear-sky levels (i.e., the daily total time in minutes that the CMF is higher than 1.1). Cloud enhancement events at Chajnantor last on average by 12 min in total per day.

northern Africa (Cordero et al. 2018a). These relatively low TOC values alone account for up to 20% of the differences between the erythemally active UV irradiances measured in the Atacama Desert and in northern Africa.

The highest UV irradiances measured at Chajnantor are associated with cloud enhancement events. Attributable to broken cloud conditions, the daily maximum UV index at Chajnantor frequently exceeds the clear-sky ceiling. For example, on 22 January 2020 we measured the highest surface UV index ever registered under quality-controlled conditions (Fig. 4c). In the case of the UV spectrum, quality-controlled measurements require a double monochromator-based spectroradiometer; we used a Bentham DMC300, which required
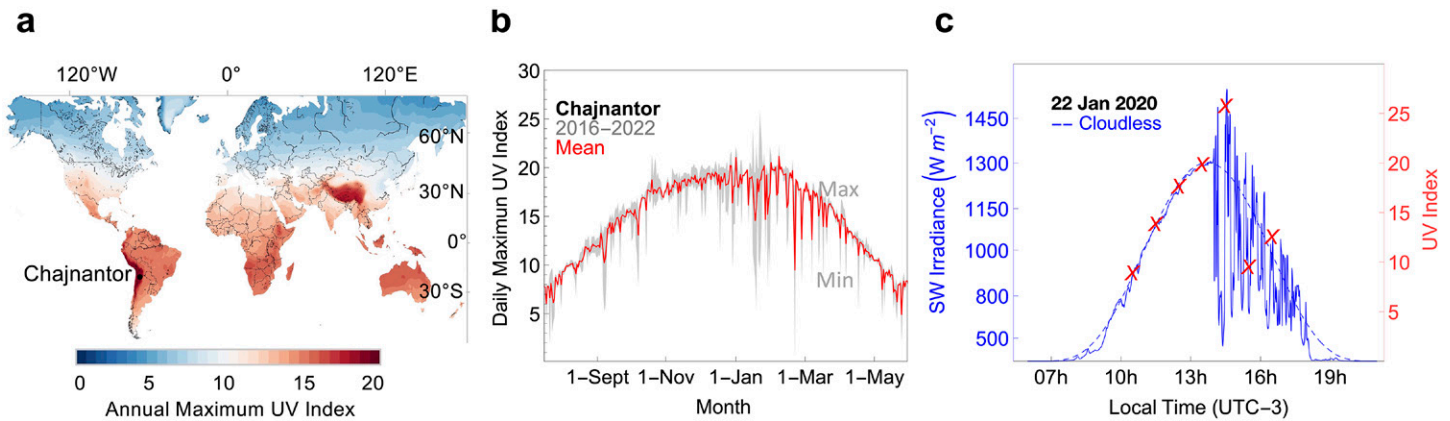
Fig. 4. Cloud enhancement also leads to extremes in the UV irradiance. (a) Annual maximum UV index averaged over the period 2011–20. The data were obtained from the global gridded Aura-OMI Spectral Surface UVB Irradiance and Erythemal Dose product (OMUVBd). According to satellite estimates the annual maximum UV index at Chajnantor is slightly lower than 20. (b) Daily maximum UV index measured at Chajnantor using a double monochromator-based Bentham DMC300 spectroradiometer. The gray shading indicates the highest and lowest values measured for each day of year (DOY) over the period 2016–22 while the red line indicates the mean over the same period. Likely due to cloud enhancement events, our measurements at Chajnantor show that the daily maximum UV index often exceeds 20. (c) Ground-based measurements at Chajnantor on 22 Jan 2020: 1-min all-sky SW irradiance (solid blue line), clear-sky SW irradiance computed using a radiative transfer model (dashed blue line), and 1-h all-sky UV index (red crosses). Our measurements at Chajnantor show that scattering by broken clouds around noon led to all-sky irradiances (both SW and UV) far exceeding clear-sky levels. On 22 Jan 2020, the UV index peaked at 25.8, which is the world's highest value ever registered by using a double-monochromator-based spectroradiometer.

more than 1 min to scan the UV spectrum. Due to the scanning time and the limited temporal resolution of our spectral measurements (1-h resolution), we may have missed some UV records associated with short-lived cloud enhancement events. In other words, the UV record in Fig. 4c is hardly the maximum possible UV index on the Chajnantor Plateau. Additional examples of cloud-driven UV extremes are shown in Fig. S7. For comparison, at the Izaña Observatory (2,367 m MSL, 28°18′N, 16°30′W, Tenerife Island), the annual maximum UV index peaks at about 14 (Cordero et al. 2013). The World Health Organization considers that values of the UV index greater than 11 indicate extreme risk of harm from unprotected sun exposure (Zaratti et al. 2014).

Discussion and conclusions

The Altiplano of the Atacama Desert is the most irradiated place on Earth. Due to its proximity to the equator, the annual irradiation (i.e., the annual dose) is far higher (more than 20%) on the Chajnantor Plateau than in other high-altitude regions like the Tibetan Plateau. Despite the higher elevation of the peaks on the Tibetan Plateau, our measurements suggest that annual maximum SW irradiances are on average also slightly higher at Chajnantor than at South Col, close to the summit of Mount Everest.

Surface SW extremes registered on the Chajnantor Plateau are unparalleled worldwide. The unique features of the Chajnantor Plateau include the strong forward scattering by broken clouds that often makes SW irradiance far exceed the clear-sky ceiling. Our measurements show that these transient cloud enhancement events occur on the Chajnantor Plateau at a frequency, intensity, and duration not previously seen anywhere in the world. Attributable to cloud enhancements, 7 of the highest 10 SW extremes on record around the world were registered on the Chajnantor Plateau (Table 1). SW extremes associated with cloud enhancement events are so recurrent at Chajnantor that the daily maximum SW irradiance exceeds on average extraterrestrial levels during much of the summer (Fig. 1d). While enhancement events (exceeding, for example, 1,100 W m^{-2}) lasted up to 420 s elsewhere (Lappalainen and Kleissl 2020), we have registered at Chajnantor events of similar intensity that lasted several hours (Fig. 3b).

Surface SW extremes on the Chajnantor Plateau are driven by clouds. Occasional albedo enhancements triggered by snowfalls are several times lower than cloud enhancements. Although the Atacama Desert is one of the driest regions on Earth, the South American monsoon (Carvalho et al. 2012) brings convective precipitation (in the form of snow) to the Chajnantor Plateau during the austral summer (Cordero et al. 2019). The rest of the year, clouds are associated with passing frontal systems (and cutoff lows) (Garreaud and Aceituno 2007). Snowfall occasionally boosts the already high albedo of the Atacama Desert (Cordero et al. 2021), especially in winter. Due to lower temperatures, snow persistence on the Chajnantor Plateau peaks in early July (Fig. S8). However, snow on Chajnantor is generally thin and patchy (Cordero et al. 2019) such that albedo enhancements (up to 1.05) generally play a limited role in the surface SW extremes. Cloud enhancements close to the 1.8 [the upper limit suggested by models (Yordanov et al. 2015)] have been registered at Chajnantor.

Cloud enhancement at Chajnantor does not increase the solar energy potential. Despite the intense, long, and frequent cloud enhancement events, they are unable to push daily irradiation beyond the clear-sky ceiling and daily CMF values at Chajnantor always remain below 1 (Fig. 3a). The fact that daily CMF values remain below 1 underlines the transient nature of cloud enhancement events. According to our measurements, cloud attenuation prevails over cloud enhancement when it comes to solar energy potential.

Cloud enhancement does boost the surface SW variability and in turn exacerbate the intermittency of photovoltaic (PV) power plants (Lappalainen and Kleissl 2020; Järvelä et al. 2020). The limitations of inverters to respond to periods of enhanced variability could result in reliability concerns including frequency violations. The rapid passage from cloud attenuation to cloud enhancement may result in large power ramp rates (Tapakis and Charalambides 2014; Inman et al. 2016). Large ramp rates can cause voltage flickers that in turn trigger tap chargers on distribution feeders increasing operations cost and the need of grid stabilization services (Tapakis and Charalambides 2014; Inman et al. 2016). The frequent and intense cloud enhancement events make the Chajnantor Plateau an ideal place for testing safety, durability, and design of future variability-proof PV power plants.

Data availability statement. NASA's CERES Energy Balanced and Filled (EBAF) data are available at https://asdc.larc.nasa.gov/project/CERES/CERES_EBAF_Edition4.1. OMI-DOAS ozone data are available at https://disc.gsfc.nasa.gov/datasets/OMDOAO3e_003/summary. Level-3 MYD08_M3 – MODIS/Aqua Aerosol Cloud Water Vapor Ozone Monthly L3 Global datasets are available at https://ladsweb.modaps.eosdis.nasa.gov/missions-and-measurements/products/MYD08_M3#overview. M2TMNXCSP (or tavgM_2d_csp_Nx) data, including the MODIS cloud fraction total mean, are available at https://disc.gsfc.nasa.gov/datasets/M2TMNXCSP_5.12.4/summary. OMUVBd products of the global erythemally weighted daily dose and erythemal dose rate are available at https://disc.gsfc.nasa.gov/datasets/OMUVBd_003/summary. *GOES-16* images are available at http://satelite.cptec.inpe.br. All ground-based measurements on the Chajnantor Plateau created or used during this study are openly available at http://antarctica.cl/wp/wp-content/uploads/2022/10/Chajnantor-ground-based-measurements.zip.

Appendix A: Satellite data

Estimates of the 1° surface SW irradiance for 2011–20 (Fig. 1b) are from the NASA's CERES Energy Balanced and Filled (EBAF) data (NASA/LARC/SD/ASDC 2019); datasets are available at https://asdc.larc.nasa.gov/project/CERES/CERES_EBAF_Edition4.1. The satellite-derived CERES-EBAF data are used for climate model evaluation and for estimating the Earth's global mean energy budget. The CERES project has launched seven instruments including flight models 1 and 2 (FM1 and FM2) on *Terra* in December 1999, FM3 and FM4 on *Aqua* in May 2002, FM5 on the *Suomi National Polar-Orbiting Partnership* (*Suomi NPP*) in October 2011, and FM6 on the *Joint Polar Satellite System-1* (*JPSS-1*)/*NOAA-20* in November 2017 (Kratz et al. 2020). Estimates from *Terra* and *Aqua* instruments constitute the longest data record and have undergone the most extensive characterization and calibration (Loeb et al. 2016). Comparison between surface-measured and CERES-derived clear-sky SW fluxes shows differences of about 2.4% from all surface types combined (Kratz et al. 2020).

Ozone data (Fig. 2a) are from the Ozone Monitoring Instrument (OMI) Differential Optical Absorption Spectroscopy (OMI-DOAS) on board the *Aura* satellite (Veefkind 2012), available at https://disc.gsfc.nasa.gov/datasets/OMDOAO3e_003/summary. Validation efforts of these products have been primarily based on comparisons with a network of Dobson and Brewer ground stations. OMI-DOAS estimates are on average only about 1.1% higher than measurements conducted at 76 ground-based stations (McPeters et al. 2008).

Estimates of aerosols (Fig. 2b) and precipitable water (Fig. 2c) are from the level-3 Moderate Resolution Imaging Spectroradiometer (MODIS) on board the *Aqua* satellite. Specifically, we used the 1° resolution MYD08_M3–MODIS/Aqua Aerosol Cloud Water Vapor Ozone Monthly L3 Global dataset (Platnick et al. 2015) available at https://ladsweb.modaps.eosdis.nasa.gov/missions-and-measurements/products/MYD08_M3#overview. All level-3 MODIS atmosphere monthly global parameters are derived from the scientific parameters of MODIS Atmosphere Daily Global Joint Product (MYD08_D3).

Cloud fraction data (Fig. S6) are from Modern-Era Retrospective Analysis for Research and Applications version 2 (MERRA-2), produced by the Goddard Earth Observing System Data Assimilation System (GEOS DAS) using the Goddard Earth Observing System Model (GEOS) version 5.12.4 (GMAO 2015). Specifically, we used the M2TMNXCSP (or tavgM_2d_csp_Nx), which is a time-averaged two-dimensional monthly mean data collection including the MODIS cloud fraction total mean. Datasets are available at https://disc.gsfc.nasa.gov/datasets/M2TMNXCSP_5.12.4/summary.

Monthly mean of satellite-derived estimates of the snow persistence are from MODIS/*Terra* Snow Cover Daily L3 Global 500m SIN Grid, version 6 (Hall and Riggs 2016). Datasets are available at https://nsidc.org/data/MOD10A1/versions/6.

For satellite-retrieved estimates (under cloudless conditions) of the UV index (Fig. 4a), we used the level-3 daily global gridded *Aura*-OMI Spectral Surface UVB Irradiance and Erythemal Dose product (OMUVBd) (Hovila et al. 2013). The OMUVBd product contains global erythemally weighted daily dose and erythemal dose rate at local solar noon at 1.0° × 1.0° grids. Data are available at https://disc.gsfc.nasa.gov/datasets/OMUVBd_003/summary.

Appendix B: Ground-based measurements

Ground-based measurements have been conducted since 2016 at the Chajnantor atmospheric observatory (5,148 m MSL, 22.95°S, 67.78°W, Chile) located at the northwestern border of the Chajnantor Plateau (Fig. S3). Measurements at Chajnantor are made to determine baseline levels, trends, and causes of variability of the surface solar irradiance and

several atmospheric gases (including ozone and the water vapor). The Chajnantor observatory contributes to international networks such as the following:

- AERONET (Aerosol Robotic Network), which provides globally distributed observations of spectral AOD, inversion products, and TPW (Holben 1998). The measurements for AERONET are carried out using a Cimel photometer model CE318-TS9 that allows estimating the TPW column as well as the AOD at the following wavelengths: 340, 380, 440, 500, 675, 870, 1,020, and 1,640 nm.
- EUBREWNET (European Brewer network), which coordinates Brewer spectrophotometer measurements of ozone, spectral UV, and the AOD in the UV part of the spectrum (AOD-UV) in Europe and beyond (Rimmer et al. 2018).
- SKYNET, a network focused on the aerosol–cloud–solar radiation interaction (Nakajima et al. 2020). The measurements for SKYNET are carried out using a Prede photometer model POM-01 that allows estimating the AOD at the following wavelengths: 400, 440, 500, 675, 870, and 1,020 nm.

Measurements of the SW irradiance at Chajnantor (Figs. 1c,d) at 1-min resolution were conducted using a SMP21 Kipp and Zonen pyranometer, which is an ISO 9060 spectrally flat Class A pyranometer (the highest-possible ISO pyranometer performance category). The instrument combines a thermopile-based sensor with a RS-485 Modbus interface, which amplifies analog output and improves the response time (less than 2 s). The SMP21 unit is protected against overvoltage, reversed polarity, and short circuiting (www.kippzonen.com/Product/359/SMP21-Pyranometer#.YpDDUi-B3T0). The pyranometer is fitted with a CVF4 ventilation unit aimed at reducing dome soiling by dust and dirt and reducing thermal offsets by stabilizing the temperature (www.kippzonen.com/Product/262/CVF4-Ventilation-Unit#.YpDE3i-B3T0). Separated studies (e.g., Cordero et al. 2018b) have estimated soiling-related annual energy losses of 3% or less at high-altitude sites in Atacama Desert. Monthly or weekly losses are accordingly much lower. Despite the relatively low local soiling, cleaning of the dome has been conducted every 2–4 weeks. In accordance with prior efforts specifically aimed at evaluating the uncertainty of pyranometers (e.g., Myers et al. 2004), the uncertainties associated with our broadband measurements are estimated to be lower than 3%, also in the case of the extremely high irradiances resulting from cloud enhancement events. Calibrations of the instrument have been conducted every 2 years following the ISO 9846 norm (www.iso.org/standard/17724.html), recommended for the calibration of pyranometers used as reference instruments. As calibration standard, we use an absolute cavity radiometer traceable to the World Radiation Center (WRC, Davos).

Measurements of the surface solar spectrum (290–1,800 nm) at 1-h resolution on the Chajnantor Plateau were carried out using a spectroradiometer system that fulfills specifications of the Network for the Detection of Atmospheric Composition Change (NDACC) (Wuttke et al. 2006) and the World Meteorological Organization (WMO) (Seckmeyer et al. 2001). The system is based on a double monochromator Bentham DMC300 (300 mm focal length) fitted with a photomultiplier detector (especially important in the UV range), a Silicon photodiode detector, and an InGaAs detector for measurements at wavelength longer that 1,100 nm. The Full Width at Half Maximum (FWHM) of the spectroradiometer is 1 nm over the range 290–650 nm and 5 nm over the range 650–1,800 nm. An integrating sphere fitted with a quartz dome is used as input optics; cleaning of the dome is conducted every 2–4 weeks. Although sampling the UV spectrum (290–400 nm) may take only a couple of minutes, the scan over the range 290–1,800 nm takes about 9 min. The spectroradiometer renders spectral measurements with uncertainties of up to 10% in the case of UV-B wavelengths (290–315 nm) and up to 4% in the case of longer wavelengths (Cordero et al. 2008).

Calibrations of the instrument have been conducted every 4–6 weeks following the WMO-GAW 125 recommendations (Seckmeyer et al. 2001). As a calibration standard, halogen lamps traceable to the Physikalisch-Technische Bundesanstalt (PTB, Germany) are used.

The UV-A and UV-B irradiance as well as the photosynthetically active radiation (PAR) were computed from the measurements of the global solar spectrum by calculating the integral within the ranges 315–400, 290–315, and 400–700 nm, respectively. The results are shown in Fig. S9. The erythemal irradiance was computed by calculating the integral of the spectral UV irradiance in the range 250–400 nm, weighted by the so-called McKinlay–Diffey erythema action spectrum (McKinlay and Diffey 1987). The dimensionless values of the UV index (shown in Figs. 4b,c) were obtained by scaling the erythemal irradiance using the factor 40 m^2 W^{-1}.

Additional comparisons involved estimates by the libRadtran software package for radiative transfer calculations (Mayer and Kylling 2005). This radiative transfer model uses the Discrete Ordinates Radiative Transfer (DISORT) solver (Dahlback and Stamnes 1991) and the extraterrestrial spectrum by Gueymard (2004). When the atmospheric composition (TOC, TPW, and AOD) is available, this model can estimate the cloud-free spectral irradiance with relatively high accuracy (Fig. S10). In the UV spectral range, the model has been validated by systematic comparisons with ground-based measurements under cloudless conditions (Badosa et al. 2007; Satheesh et al. 2006). Under cloudless conditions, the libRadtran model renders spectral measurements with uncertainties of up to 15% in the case of UV-B wavelengths (290–315 nm) (Cordero et al. 2007), and up to 6% in the case of longer wavelengths (Belluardo et al. 2016). Systematic comparisons with model outputs allowed retrieval of estimates of TOC and TPW from our ground-based spectral measurements.

Appendix C: Analysis of extremes

In the case of the results shown in Figs. 3d–f, we applied a methodology widely used for computing the probability of extreme events (e.g., Feron et al. 2021, and references therein).

First, we analyzed the extremes in the SW irradiances. For each day of year (DOY), we used 29-day rolling windows to form datasets of daily maximum surface SW irradiance measured at Chajnantor over the period 2016–22. This means that, over a 5-yr period, we formed datasets of up to 145 (29 × 5 = 145) measurements for each DOY. As an example, histograms of the datasets corresponding to the DOY = 1 (1 January) and to the DOY = 305 (1 November) are shown in Fig. S11a. Similar histograms (or the corresponding probability density functions) for each DOY allowed us to compute the probability of the daily maximum surface SW irradiance at Chajnantor being higher than the TSI (Fig. 3d).

Second, we analyzed the statistics of the cloud enhancement events (i.e., when the all-sky SW irradiance exceeds clear-sky levels by at least 10%). We calculated the 1-min-resolution cloud modification factor (CMF) dividing our all-sky SW measurements at Chajnantor over the period 2016–22 by the corresponding clear-sky SW irradiance computed using the libRadtran software package for radiative transfer calculations (Mayer and Kylling 2005). Then, for each DOY, we used 29-day rolling windows to form datasets of the daily maximum CMF. This means that, over a 5-yr period, we formed datasets of up to 145 (29 × 5 = 145) CMF values for each DOY. As an example, the histograms of the datasets corresponding to the DOY = 1 (1 January) and to the DOY = 305 (1 November) are shown in Fig. S11b. Similar histograms (or the corresponding probability density functions) for each DOY allowed us to compute the probability of the daily maximum CMF at Chajnantor being higher than 1.1 (Fig. 3d), which is equivalent to the probability of the all-sky SW values being at least 10% higher than clear-sky levels for at least 1 min. The mean and the median of the datasets corresponding to each DOY are shown in Fig. 3e.

Finally, we analyzed the statistics of the cloud enhancement duration. We calculated the number of minutes per day that our all-sky SW measurements over the period 2016–22 were at least 10% higher than clear-sky level (i.e., the daily total time in minutes that the CMF was higher than 1.1). Then, for each DOY, we used 29-day rolling windows to form datasets of the daily cloud enhancement duration. This means that, over a 5-yr period, we formed datasets of up to 145 (29 × 5 = 145) values for each DOY. As an example, the histograms of the datasets corresponding to the DOY = 1 (1 January) and to the DOY = 305 (1 November) are shown in Fig. S11c. Similar histograms (or the corresponding probability density functions) for each DOY allowed us to compute the mean and the median of the cloud enhancement duration (Fig. 3f).

References

Aliaga, D., and Coauthors, 2021: Identifying source regions of air masses sampled at the tropical high-altitude site of Chacaltaya using WRF-FLEXPART and cluster analysis. *Atmos. Chem. Phys.*, **21**, 16453–16477, https://doi.org/10.5194/acp-21-16453-2021.

Almeida, M. P., R. Zilles, and E. Lorenzo, 2014: Extreme overirradiance events in São Paulo, Brazil. *Sol. Energy*, **110**, 168–173, https://doi.org/10.1016/j.solener.2014.09.012.

Badosa, J., R. L. McKenzie, M. Kotkamp, J. Calbo, and J. A. Gonzalez, 2007: Towards closure between measured and modelled UV under clear skies at four diverse sites. *Atmos. Chem. Phys.*, **7**, 2817–2837, https://doi.org/10.5194/acp-7-2817-2007.

Belluardo, G., G. Barchi, D. Baumgartner, M. Rennhofer, P. Weihs, and D. Moser, 2016: Uncertainty analysis of a radiative transfer model using Monte Carlo method within 280–2500 nm region. *Sol. Energy*, **132**, 558–569, https://doi.org/10.1016/j.solener.2016.03.050.

Carvalho, L. M., C. Jones, A. N. Posadas, R. Quiroz, B. Bookhagen, and B. Liebmann, 2012: Precipitation characteristics of the South American monsoon system derived from multiple datasets. *J. Climate*, **25**, 4600–4620, https://doi.org/10.1175/JCLI-D-11-00335.1.

Castillejo-Cuberos, A., and R. Escobar, 2020: Detection and characterization of cloud enhancement events for solar irradiance using a model-independent, statistically-driven approach. *Sol. Energy*, **209**, 547–567, https://doi.org/10.1016/j.solener.2020.09.046.

Cede, A., M. Blumthaler, E. Luccini, R. D. Piacentini, and L. Nuñez, 2002: Effects of clouds on erythemal and total irradiance as derived from data of the Argentine Network. *Geophys. Res. Lett.*, **29**, 76-1–76-4, https://doi.org/10.1029/2002GL015708.

Collaud Coen, M., and Coauthors, 2018: Identification of topographic features influencing aerosol observations at high altitude stations. *Atmos. Chem. Phys.*, **18**, 12289–12313, https://doi.org/10.5194/acp-18-12289-2018.

Cordero, R. R., G. Seckmeyer, D. Pissulla, L. Dasilva, and F. Labbe, 2007: Uncertainty evaluation of the spectral UV irradiance evaluated by using the UVSPEC radiative transfer model. *Opt. Commun.*, **276**, 44–53, https://doi.org/10.1016/j.optcom.2007.04.008.

——, ——, ——, L. DaSilva, and F. Labbe, 2008: Uncertainty evaluation of spectral UV irradiance measurements. *Meas. Sci. Technol.*, **19**, 045104, https://doi.org/10.1088/0957-0233/19/4/045104.

——, ——, A. Damiani, S. Riechelmann, J. Rayas, F. Labbe, and D. Laroze, 2013: The world's highest levels of surface UV. *Photochem. Photobiol. Sci.*, **13**, 70–81, https://doi.org/10.1039/c3pp50221j.

——, and Coauthors, 2016: The solar spectrum in the Atacama Desert. *Sci. Rep.*, **6**, 22457, https://doi.org/10.1038/srep22457.

——, and Coauthors, 2018a: Ultraviolet radiation in the Atacama Desert. *Antonie van Leeuwenhoek*, **111**, 1301–1313, https://doi.org/10.1007/s10482-018-1075-z.

——, and Coauthors, 2018b: Effects of soiling on photovoltaic (PV) modules in the Atacama Desert. *Sci. Rep.*, **8**, 13943, https://doi.org/10.1038/s41598-018-32291-8.

——, and Coauthors, 2019: Dry-season snow cover losses in the Andes (18°–40°S) driven by changes in large-scale climate modes. *Sci. Rep.*, **9**, 16945, https://doi.org/10.1038/s41598-019-53486-7.

——, and Coauthors, 2021: Evaluation of MODIS-derived estimates of the albedo over the Atacama Desert using ground-based spectral measurements. *Sci. Rep.*, **11**, 19822, https://doi.org/10.1038/s41598-021-98622-4.

Dahlback, A., and K. Stamnes, 1991: A new spherical model for computing the radiation field available for photolysis and heating at twilight. *Planet. Space Sci.*, **39**, 671–683, https://doi.org/10.1016/0032-0633(91)90061-E.

Damiani, A., and Coauthors, 2018: Evaluation of Himawari-8 surface downwelling solar radiation by ground-based measurements. *Atmos. Meas. Tech.*, **11**, 2501–2521, https://doi.org/10.5194/amt-11-2501-2018.

do Nascimento, L. R., T. de Souza Viana, R. A. Campos, and R. Rüther, 2019: Extreme solar overirradiance events: Occurrence and impacts on utility-scale photovoltaic power plants in Brazil. *Sol. Energy*, **186**, 370–381, https://doi.org/10.1016/j.solener.2019.05.008.

Dudok de Wit, T., G. Kopp, C. Fröhlich, and M. Schöll, 2017: Methodology to create a new total solar irradiance record: Making a composite out of multiple data records. *Geophys. Res. Lett.*, **44**, 1196–1203, https://doi.org/10.1002/2016GL071866.

Emck, P., and M. Richter, 2008: An upper threshold of enhanced global shortwave irradiance in the troposphere derived from field measurements in tropical mountains. *J. Appl. Meteor. Climatol.*, **47**, 2828–2845, https://doi.org/10.1175/2008JAMC1861.1.

ESMAP, 2020: Global Photovoltaic Power Potential by Country (English). World Bank Group, 48 pp., http://documents.worldbank.org/curated/en/466331592817725242/Global-Photovoltaic-Power-Potential-by-Country.

ESO, 2007: Close to the Sky: Biological Heritage of the ALMA area. ESO, 76 pp., www.eso.org/public/archives/books/pdfsm/book_0043.pdf.

Feron, S., R. R. Cordero, A. Damiani, and R. B. Jackson, 2021: Climate change extremes and photovoltaic power output. *Nat. Sustainability*, **4**, 2070–2276, https://doi.org/10.1038/s41893-020-00643-w.

Garreaud, R., and P. Aceituno, 2007: Atmospheric circulation over South America: Mean features and variability. *The Physical Geography of South America*, T. Veblen, A. Orme, and K. Young, Eds., Oxford University Press, 45–66.

Gelsor, N., N. Gelsor, T. Wangmo, Y. C. Chen, Ø. Frette, J. J. Stamnes, and B. Hamre, 2018: Solar energy on the Tibetan Plateau: Atmospheric influences. *Sol. Energy*, **173**, 984–992, https://doi.org/10.1016/j.solener.2018.08.024.

GMAO, 2015: MERRA-2 tavgM_2d_csp_Nx: 2d, monthly mean, time-averaged, single-level, assimilation, COSP Satellite Simulator V5.12.4. Goddard Earth Sciences Data and Information Services Center (GES DISC), accessed 27 May 2022, https://doi.org/10.5067/BZPOTGJOQKLU.

Gueymard, C. A., 2004: The sun's total and spectral irradiance for solar energy applications and solar radiation models. *Sol. Energy*, **76**, 423–453, https://doi.org/10.1016/j.solener.2003.08.039.

——, 2017: Cloud and albedo enhancement impacts on solar irradiance using high-frequency measurements from thermopile and photodiode radiometers. Part 1: Impacts on global horizontal irradiance. *Sol. Energy*, **153**, 755–765, https://doi.org/10.1016/j.solener.2017.05.004.

Hall, D. K., and G. A. Riggs, 2016: MODIS/terra snow cover daily L3 global 500m SIN grid, version 6. NASA National Snow and Ice Data Center Distributed Active Archive Center, accessed 6 June 2022, https://doi.org/10.5067/MODIS/MOD10A1.006.

Holben, B. N., 1998: AERONET – A federated instrument network and data archive for aerosol characterization. *Remote Sens. Environ.*, **66**, 1–16, https://doi.org/10.1016/S0034-4257(98)00031-5.

Hovila, J., A. Arola, and J. Tamminen, 2013: OMI/Aura surface UVB irradiance and erythemal dose daily L3 global gridded 1.0 degree × 1.0 degree V3. NASA Goddard Earth Sciences Data and Information Services Center (GES DISC), accessed 6 June 2022, https://doi.org/10.5067/Aura/OMI/DATA3009.

Hunter, J. D., 2007: Matplotlib: A 2D graphics environment. *Comput. Sci. Eng.*, **9**, 90–95, https://doi.org/10.1109/MCSE.2007.55.

Inman, R. H., Y. Chu, and C. F. Coimbra, 2016: Cloud enhancement of global horizontal irradiance in California and Hawaii. *Sol. Energy*, **130**, 128–138, https://doi.org/10.1016/j.solener.2016.02.011.

Jara, M. Z., H. Berg, L. A. Conde, M. A. Sevillano-Bendezú, A. M. Carhuavilca, R. Grieseler, and J. A. Töfflinger, 2021: Extreme overirradiance events and their spectral distribution in Lima, Peru. *J. Phys.*, **1841**, 012006, https://doi.org/10.1088/1742-6596/1841/1/012006.

Järvelä, M., K. Lappalainen, and S. Valkealahti, 2020: Characteristics of the cloud enhancement phenomenon and PV power plants. *Sol. Energy*, **196**, 137–145, https://doi.org/10.1016/j.solener.2019.11.090.

Kratz, D. P., S. K. Gupta, A. C. Wilber, and V. E. Sothcott, 2020: Validation of the CERES edition-4A surface-only flux algorithms. *J. Appl. Meteor. Climatol.*, **59**, 281–295, https://doi.org/10.1175/JAMC-D-19-0068.1.

Lappalainen, K., and J. Kleissl, 2020: Analysis of the cloud enhancement phenomenon and its effects on photovoltaic generators based on cloud speed sensor measurements. *J. Renewable Sustainable Energy*, **12**, 043502, https://doi.org/10.1063/5.0007550.

Loeb, N. G., N. Manalo-Smith, W. Su, M. Shankar, and S. Thomas, 2016: CERES top-of-atmosphere earth radiation budget climate data record: Accounting for in-orbit changes in instrument calibration. *Remote Sens.*, **8**, 182, https://doi.org/10.3390/rs8030182.

Marcq, S., and Coauthors, 2010: Aerosol optical properties and radiative forcing in the high Himalaya based on measurements at the Nepal Climate Observatory-Pyramid site (5079 m a.s.l.). *Atmos. Chem. Phys.*, **10**, 5859–5872, https://doi.org/10.5194/acp-10-5859-2010.

Matthews, T., and Coauthors, 2020: Going to extremes: Installing the world's highest weather stations on Mount Everest. *Bull. Amer. Meteor. Soc.*, **101**, E1870–E1890, https://doi.org/10.1175/BAMS-D-19-0198.1.

Mayer, B., and A. Kylling, 2005: Technical note: The libRadtran software package for radiative transfer calculations – Description and examples of use. *Atmos. Chem. Phys.*, **5**, 1855–1877, https://doi.org/10.5194/acp-5-1855-2005.

McKinlay, A., and B. Diffey, 1987: A reference action spectrum for ultraviolet induced erythema in human skin. *CIE J.*, **6**, 17–22.

McPeters, R., and Coauthors, 2008: Validation of the Aura Ozone Monitoring Instrument total column ozone product. *J. Geophys. Res.*, **113**, D15S14, https://doi.org/10.1029/2007JD008802.

Myers, D. R., I. M. Reda, S. M. Wilcox, and T. L. Stoffel, 2004: Uncertainty analysis for broadband solar radiometric instrumentation calibrations and measurements: An update. *World Renewable Energy Congress VIII*, Denver, CO, NREL, 8 pp., www.nrel.gov/docs/fy04osti/36201.pdf.

Nakajima, T., and Coauthors, 2020: An overview of and issues with sky radiometer technology and SKYNET. *Atmos. Meas. Tech.*, **13**, 4195–4218, https://doi.org/10.5194/amt-13-4195-2020.

NASA/LARC/SD/ASDC, 2019: CERES Energy Balanced and Filled (EBAF) TOA and surface monthly means data in netCDF edition 4.1. NASA Langley Atmospheric Science Data Center DAAC, accessed 31 May 2022, https://doi.org/10.5067/TERRA-AQUA/CERES/EBAF_L3B.004.1.

Pfister, G., R. L. McKenzie, J. B. Liley, A. Thomas, B. W. Forgan, and C. N. Long, 2003: Cloud coverage based on all-sky imaging and its impact on surface solar irradiance. *J. Appl. Meteor.*, **42**, 1421–1434, https://doi.org/10.1175/1520-0450(2003)042<1421:CCBOAI>2.0.CO;2.

Piacentini, R. D., A. Cede, and H. Bárcena, 2003: Extreme solar total and UV irradiances due to cloud effect measured near the summer solstice at the high-altitude desertic plateau Puna of Atacama (Argentina). *J. Atmos. Sol.-Terr. Phys.*, **65**, 727–731, https://doi.org/10.1016/S1364-6826(03)00084-1.

——, G. M. Salum, N. Fraidenraich, and C. Tiba, 2011: Extreme total solar irradiance due to cloud enhancement at sea level of the NE Atlantic coast of Brazil. *Renewable Energy*, **36**, 409–412, https://doi.org/10.1016/j.renene.2010.06.009.

Piedehierro, A. A., M. Antón, A. Cazorla, L. Alados-Arboledas, and F. J. Olmo, 2014: Evaluation of enhancement events of total solar irradiance during cloudy conditions at Granada (southeastern Spain). *Atmos. Res.*, **135–136**, 1–7, https://doi.org/10.1016/j.atmosres.2013.08.008.

Platnick, S., P. Hubanks, K. Meyer, and M. D. King, , 2015: MODIS atmosphere L3 monthly product. NASA MODIS Adaptive Processing System, Goddard Space Flight Center, accessed 27 May 2022, http://doi.org/10.5067/MODIS/MOD08_M3.006.

Prăvălie, R., C. Patriche, and G. Bandoc, 2019: Spatial assessment of solar energy potential at global scale. A geographical approach. *J. Cleaner Prod.*, **209**, 692–721, https://doi.org/10.1016/j.jclepro.2018.10.239.

Rimmer, J. S., A. Redondas, and T. Karppinen, 2018: EuBrewNet–A European Brewer network (COST Action ES1207), an overview. *Atmos. Chem. Phys.*, **18**, 10 347–10 353, https://doi.org/10.5194/acp-18-10347-2018.

Rondanelli, R., A. Molina, and M. Falvey, 2015: The Atacama surface solar maximum. *Bull. Amer. Meteor. Soc.*, **96**, 405–418, https://doi.org/10.1175/BAMS-D-13-00175.1.

Rutan, D. A., S. Kato, D. R. Doelling, F. G. Rose, L. T. Nguyen, T. E. Caldwell, and N. G. Loeb, 2015: CERES synoptic product: Methodology and validation of surface radiant flux. *J. Atmos. Oceanic Technol.*, **32**, 1121–1143, https://doi.org/10.1175/JTECH-D-14-00165.1.

Satheesh, S. K., J. Srinivasan, V. Vinoj, and S. Chandra, 2006: New directions: How representative are aerosol radiative impact assessments? *Atmos. Environ.*, **40**, 3008–3010, https://doi.org/10.1016/j.atmosenv.2006.01.031.

Seckmeyer, G., A. Bais, G. Bernhard, M. Blumthaler, and C. R. Booth, 2001: Instruments to measure solar ultraviolet radiation. Part 1: Spectral. WMO-GAW 125, 36 pp., https://library.wmo.int/doc_num.php?explnum_id=9182.

Staiger, H., P. N. Den Outer, A. F. Bais, U. Feister, B. Johnsen, and L. Vuilleumier, 2008: Hourly resolved cloud modification factors in the ultraviolet. *Atmos. Chem. Phys.*, **8**, 2493–2508, https://doi.org/10.5194/acp-8-2493-2008.

Tapakis, R., and A. G. Charalambides, 2014: Enhanced values of global irradiance due to the presence of clouds in eastern Mediterranean. *Renewable Energy*, **62**, 459–467, https://doi.org/10.1016/j.renene.2013.08.001.

Veefkind, P., 2012: OMI/Aura Ozone (O3) DOAS total column L3 1 day 0.25 degree × 0.25 degree V3. Goddard Earth Sciences Data and Information Services Center (GES DISC), accessed 27 May 2022, https://doi.org/10.5067/Aura/OMI/DATA3005.

Wei, J., Y. Peng, J. Guo, and L. Sun, 2019: Performance of MODIS Collection 6.1 Level 3 aerosol products in spatial-temporal variations over land. *Atmos. Environ.*, **206**, 30–44, https://doi.org/10.1016/j.atmosenv.2019.03.001.

Wuttke, S., G. Seckmeyer, G. Bernhard, J. Ehramjian, and R. McKenzie, 2006: New spectroradiometers complying with the NDSC standards. *J. Atmos. Oceanic Technol.*, **23**, 241–251, https://doi.org/10.1175/JTECH1826.1.

Yang, D., and J. M. Bright, 2020: Worldwide validation of 8 satellite-derived and reanalysis solar radiation products: A preliminary evaluation and overall metrics for hourly data over 27 years. *Sol. Energy*, **210**, 3–19, https://doi.org/10.1016/j.solener.2020.04.016.

Yordanov, G. H., T. O. Saetre, and O. M. Midtgård, 2015: Extreme overirradiance events in Norway: 1.6 suns measured close to 60°N. *Sol. Energy*, **115**, 68–73, https://doi.org/10.1016/j.solener.2015.02.020.

Zaratti, F., R. D. Piacentini, H. A. Guillén, S. H. Cabrera, J. B. Liley, and R. L. McKenzie, 2014: Proposal for a modification of the UVI risk scale. *Photochem. Photobiol. Sci.*, **13**, 980–985, https://doi.org/10.1039/c4pp00006d.